Dynamics of spatiotemporally propagating transport barriers

P. H. Diamond[a] and V. B. Lebedev
University of California at San Diego, La Jolla, California 92093-0319

D. E. Newman and B. A. Carreras
Oak Ridge National Laboratory, Oak Ridge, Tennessee 37831-8070

(Received 9 January 1995; accepted 6 June 1995)

A simple dynamic model of spatiotemporally propagating transport barriers and transition fronts from low (L) to high (H) confinement regimes is presented. The model introduces spatial coupling (via transport), into the coupled evolution equations for flow shear and fluctuation intensity, thus coupling the supercritical L to H bifurcation instability to turbulent transport. Hence, fast spatiotemporal front propagation and evolutionary behavior result. The theory yields expressions for the propagation velocity and termination point of an L–H transition front and transport barrier. When the evolution of the pressure gradient, ∇P_i, and the contribution of ∇P_i to sheared electric field, E_r', is included, the ambient pretransition pressure gradient acts as a local source term that drives the evolution of the poloidal velocity shear. The transition may then evolve either as a spatiotemporally propagating front or as a uniform (i.e., nonlocal) fluctuation reduction or quench. The precise route to transition adopted depends on the relative magnitudes of the front transit time, τ_T, and the fluctuation reduction time, τ_f, respectively. The relevance of spatiotemporally propagating L–H transition fronts to the very high confinement regime (VH mode) evolution in DIII-D [R. I. Pinsker and the DIII-D Team, *Plasma Physics and Controlled Nuclear Fusion Research 1992* (International Atomic Energy Agency, Vienna, 1993), Vol. 1, p. 683] and in the Joint European Torus (JET) [*Plasma Physics and Controlled Nuclear Fusion Research 1990* (International Atomic Energy Agency, Vienna, 1991), Vol. 1, p. 27] is discussed. © *1995 American Institute of Physics.*

I. INTRODUCTION

Transient and evolutionary phenomena are frequently encountered in tokamak plasmas. Foremost among these is the transition from the low confinement regime (L mode) to the high confinement regime (H mode),[1] which results in the formation of a narrow region of enhanced confinement at the plasma edge when a critical input power is exceeded. The transport barrier development is a consequence of a local increase in the shear of the radial electric field, which reduces and quenches turbulence via enhanced eddy decorrelation.[2] Heat, particle, and poloidal and toroidal angular momentum transport, as well as ion orbit loss,[3] contribute to the evolution of the sheared radial electric field. Thus, the width of the H-mode transport barrier is set by some combination of the turbulent correlation length, neutral penetration depth, and the ion poloidal gyroradius. Ongoing experimental and theoretical research is focused on clarifying the relative contributions of these various mechanisms and length scales to the spatial extent of the observed enhanced confinement region.[4]

Recently, a novel confinement regime in tokamaks, called the very high confinement mode (VH mode),[5,6] was discovered. The striking feature of the VH mode is that while the region of enhanced confinement and increased electric field shear is initiated at the plasma edge ($0.9 \leqslant \rho \leqslant 1.0$, where ρ is the normalized radius of a flux surface), it proceeds to develop and propagate radially inward, eventually occupying the region $\rho > 0.6$. The VH mode thus results in significantly greater enhancement of stored energy content than the H mode does, and is thus of great interest to the fusion program. From a scientific perspective, the VH mode broadens our concept of the L–H transition mechanism by demonstrating that the transport barrier may be delocalized and decoupled from the plasma boundary, and that the transition may propagate in space and time. Indeed, the discovery of the VH mode directly challenges theory to produce a model of a spatiotemporally propagating L–H transition front, in contrast to the spatially local transition paradigm advanced to date. Moreover, the discovery of the VH mode establishes that proximity to the plasma boundary is not intrinsic to confinement improvement transitions. The spatial propagation of the transition naturally introduces a new time scale, associated with the inward propagation of the enhanced confinement zone. This rapid time scale will quite likely enter the description of H- to VH-mode evolution. Moreover, the dynamic limitations on transition front propagation are likely to yield clues as to the mechanism and parameters that govern the ultimate saturation of the VH mode.

Our interest in VH-mode phenomena has been further whetted by the discovery of VH-mode confinement regimes in the Joint European Torus (JET)[6] and in TUMAN-3,[7] and by the discovery of an internal transport barrier in JT-60U.[8] The appearance of the VH mode in JET is significant, because there the plasma is heated by ion cyclotron waves (ICRF). Hence, while sheared toroidal velocity, V_ϕ', produced by neutral beam injection (NBI) may be the dominant contributor to E_r' in the DIII-D VH mode, it does not appear that V_ϕ' is intrinsic to, or necessary for, VH-mode confinement regimes. Also, in contrast to the case of DIII-D, the evolution of VH-mode profiles in JET is quite rapid. Indeed, it seems that a sudden, radially nonlocal profile jump occurs

[a]Also at General Atomics, San Diego, California.

 1070-664X/95/2(10)/3685/11/$6.00

as the discharge transitions into the VH mode. The TUMAN-3 VH-mode is of interest because the heating is entirely Ohmic. Indeed, the only feature common to DIII-D, JET, and TUMAN-3 is the need for careful wall conditioning by boronization, etc., in order to access VH-mode regimes. The JT-60U internal transport barrier is of interest on account of its "inside-out" development (i.e., from the core outward), which is in distinct contrast to the "outside-in" development (i.e., from the edge inward) characteristic of the VH mode. All these observations suggest that spatiotemporally propagating L–H transitions are dynamic phenomena intrinsic to turbulent plasmas. They also suggest the following specific questions:

(1) What is the mechanism of VH-mode buildup? (2) How can the spatiotemporal propagation of a transport barrier be described and understood? What constitutes a minimal model? (3) What roles do averaged poloidal sheared velocity, $\langle V_\theta \rangle'$; averaged diamagnetic sheared velocity, $\langle V_d \rangle'$; and sheared toroidal velocity, V_ϕ' play? Is V_ϕ' necessary for propagating transport barriers and VH mode? (4) What constitutes the "seed" for the VH-mode electric field? (5) What determines the spatial extent of enhanced confinement regime? We shall attempt to answer these questions in the following.

In this paper, a simple dynamic model of spatiotemporally propagating transport barriers and L–H transition fronts is presented. The model introduces spatial coupling into the coupled evolution equations for flow shear (via transport, i.e., turbulent viscosity) and fluctuation intensity (via nonlinear interaction), thus coupling the supercritical L–H bifurcation instability to turbulent transport. Hence, spatiotemporal front propagation and fast evolutionary behavior result. Just as the paradigm for the local L–H transition is the predator–prey model[9] (with the radial electric field shear, E_r', as predator and fluctuation intensity as prey), an epidemic propagation model (with E_r' playing the role of disease and fluctuation intensity analogous to the susceptible population) is the natural paradigm for the spatiotemporally propagating L–H transition front. This type of model has been used to study the epidemiology of the Black Death and other communicable diseases.[10] Such a model defines a second transition evolution time scale—namely, the front transit time—which is a hybrid of the local L–H bifurcation instability growth rate and a diffusive time scale, i.e., $\tau_T = L_\perp / V_F$, where $V_F \approx 2(W/L_\perp)(W\gamma_0)\sqrt{\Delta\epsilon}$ is the front propagation velocity, $L_\perp$ is the profile scale length, W is the characteristic radial scale length of the turbulence, and γ_0 is the linear growth rate. The parameter $\Delta\epsilon$ is a measure of the criticality that will be explicitly defined in Sec. III.

From the perspective of this model, a spatially localized seed flow at the edge (due to ion orbit loss, for example) could trigger an L–H transition front that propagates through the region, which is locally unstable to the L–H bifurcation, i.e., the region with $\Delta\epsilon > 0$. Note, then, that the spatial extent of the enhanced confinement zone is determined by $\Delta\epsilon(r)$, and thus by the pretransition profiles. The theory yields expressions for the propagation velocity and the termination point of the transition front. The simple two-field L–H transition model[9] can also be expanded to include pressure gradient evolution and the contribution of ∇P_i to E_r'.[11] In contrast to the simpler model, the ambient pretransition pressure gradient acts as a local source term that drives the evolution of the poloidal velocity shear. Thus, the transition may evolve either as (i) a spatiotemporally propagating front, as discussed above, or as (ii) a uniform (i.e., nonlocal) fluctuation reduction or even a fluctuation quench. It is worthwhile to point out that the front propagation is initialized by a small, strongly supercritical (to the L–H transition) region at the edge. This triggers a propagating transition front that then moves into a weakly supercritical core. The strongly supercritical edge is created by boundary effects or strong-fluctuation energy gradients—both typical of L-mode edge plasmas.

The precise route to transition the plasma will choose is a quantitative question answered by comparing the relative magnitudes of the front transit time, τ_T, and the fluctuation reduction time, τ_f, respectively. To understand the competition between these two, recall that for power levels just above the power threshold, $P \geqslant P_{\text{th}}$, the averaged poloidal sheared velocity, $\langle V_\theta \rangle'$, greatly exceeds the averaged $\mathbf{E}\times\mathbf{B}$ sheared velocity, $\langle V_E \rangle'$, with fluctuation intensity, E, close to its L-mode level, $E \leqslant 1$, while for $P \gg P_{\text{th}}$, ∇P_i dominates $\langle V_E \rangle'$ with $E \approx 0$. Thus, it is not surprising that route (i) is chosen for moderate input power levels ($\langle V_\theta \rangle' > \langle V_d \rangle'$), while route (ii) appears for high power ($\langle V_d \rangle' > \langle V_\theta \rangle'$). Thus, the qualitative nature of the route to the formation of a global VH-mode-like confinement state is seen to be a function of input power, and other parameters that determine the ratio τ_T/τ_f. This finding provides a clue to the longstanding quandary of how machine parameters determine local versus nonlocal transport and profile evolution.

The remainder of this paper is organized in the following manner. The basic, radially dependent model is derived in Sec. II. Section III contains an analysis of the L–H transition propagation in the simple flow-fluctuation model. In particular, expressions for the front propagation speed and the propagation criterion are derived and compared with numerical calculations. In Sec. IV, front dynamics in the three-field flow-fluctuation-pressure gradient model are studied numerically. The focus here is on the relative importance of front propagation and uniform fluctuation reduction mechanisms. Finally, Sec. V contains a discussion and conclusions. Special attention is given to limitations on the theory, its relevance to the VH-mode evolution, a comparison of VH-mode evolution in DIII-D and JET, and plans for future work.

II. DERIVATION OF THE NONLOCAL FLUCTUATION-FLOW MODEL

In this section, the spatially nonlocal fluctuation flow model is derived. This model is an extension of the local phase transition model for the L–H bifurcation.[9] In that model, two coupled order parameters—namely, the local poloidal flow shear $\langle V_\theta \rangle'$ and the local fluctuation intensity, $E \equiv |\tilde{n}_k/n_0|$—evolve according to the coupled equations:

$$\frac{\partial E}{\partial t} = \gamma_0 E - \alpha_1 E^2 - \alpha_2 \langle V_\theta \rangle'^2 E, \tag{1}$$

$$\frac{\partial\langle V_\theta\rangle'}{\partial t} = -\mu\langle V_\theta\rangle' + \alpha_3\langle V_\theta\rangle' E. \tag{2}$$

Here, γ_0 is the linear growth rate in the absence of sheared flow, $\hat{\mu}$ is the damping due to magnetic pumping, and the angular brackets, $\langle\ \rangle$, indicate the poloidal and the toroidal angle average over a magnetic flux surface. The coefficients α_1, α_2, and α_3 for a variety of turbulence models are given in Ref. 9. It is possible to derive generic scalings for these coefficients. Assuming that the level of fluctuations at saturation is given by the mixing length estimate, the α_1 coefficient scales as $\alpha_1 \propto (\gamma_0 L_\perp^2 / W_k^2)$. Using the turbulence suppression criterion of Biglari *et al.*,[2] it is possible to estimate α_2, $\alpha_2 \propto (\bar{k}_\theta^2 W_k^2/\gamma_0)$. In these expressions, $c_s = \sqrt{T_e/m_i}$ is the speed of sound, $\rho_s = c_s/\Omega_i$ is the sound Larmor radius, k_θ is the poloidal wave number, W_k is the radial correlation length of the turbulence, $L_\perp$ is the L-mode density scale length, and the overbar on k_θ indicates the spectral average. The coefficient α_3 has the generic scaling $\alpha_3 \propto (\sqrt{\bar{k}_\theta^2}\rho_s c_s / W_k)$.

This model may be easily extended to incorporate spatial coupling by recognizing that radial coupling occurs because of fluxes of fluctuation energy and poloidal momentum induced by the divergence-free, fluctuation-induced $\mathbf{E}\times\mathbf{B}$ flow. Hence, we immediately rewrite Eqs. (1) and (2) as

$$\frac{\partial E}{\partial t} + \frac{\partial J_E}{\partial x} = \gamma_0 E - \alpha_1 E^2 - \alpha_2\langle V_\theta\rangle'^2 E, \tag{3}$$

$$\frac{\partial\langle V_\theta\rangle'}{\partial t} + \frac{\partial J_{V'_\theta}}{\partial x} = -\hat{\mu}\langle V_\theta\rangle' + \alpha_3\langle V_\theta\rangle' E, \tag{4}$$

where J_E and $J_{V'_\theta}$ are the fluxes of fluctuation intensity and poloidal flow shear, respectively. The convective terms of Eqs. (3) and (4) clearly represent fluctuation energy advection due to nonlinear interaction and momentum convection, i.e.,

$$\left\langle \frac{-c}{B}\,\mathbf{E}\times\hat{n}\cdot\nabla\,\delta p^2 \right\rangle = \left\langle \nabla\left(\frac{-c}{B}\,\mathbf{E}\times\hat{n}(\delta p^2)\right)\right\rangle \to \frac{\partial J_E}{\partial x} \tag{5}$$

and

$$\left\langle \frac{-c}{B}\,\mathbf{E}\times\hat{n}\cdot\nabla V'_\theta \right\rangle = \left\langle \nabla\left(\frac{-c}{B}\,\mathbf{E}\times\hat{n}(V'_\theta)\right)\right\rangle \to \frac{\partial J_{V'_\theta}}{\partial x}. \tag{6}$$

The conservative structure of the fluxes follows from the incompressibility of the $\mathbf{E}\times\mathbf{B}_0$ flow. Note that Eqs. (3) and (4) constitute a generic form of the local fluctuation intensity equation (i.e., the spectrally integrated wave-kinetic equation) and the poloidal flow equation.

The spatial fluxes J_E and $J_{V'_\theta}$ must now be specified. The most general forms are

$$J_E = -D\frac{\partial E}{\partial x} + \Gamma_E^{0D} \tag{7}$$

and

$$J_{V'_\theta} = -\nu\frac{\partial\langle V_\theta\rangle'}{\partial x} + \Gamma_{V'_\theta}^{0D}, \tag{8}$$

where D is the intensity diffusivity, ν is the turbulent flow viscosity, and Γ_E^{0D}, $\Gamma_{V'_\theta}^{0D}$ are the off-diagonal contributions, respectively. Moreover, since Eqs. (1) and (2) include explicit contributions from local coupling to dissipation ($\alpha_1 E^2$) and the Reynolds stress dynamo ($\alpha_3 E\langle V_\theta\rangle'$), there is no loss of generality in setting $\Gamma_E^{0D} = \Gamma_{\theta'}^{0D} = 0$ in Eqs. (7) and (8).

Observing that the turbulence is electrostatic, we may then write

$$D \approx \nu \approx D_0 E, \tag{9}$$

where $D_0 \approx \gamma_0 W^2$. Thus, the nonlocal evolution equations are finally

$$\frac{\partial E}{\partial t} = \gamma_0 E - \alpha_1 E^2 - \alpha_2\langle V_\theta\rangle'^2 E + \frac{\partial}{\partial x}\left(D_0 E\frac{\partial E}{\partial x}\right), \tag{10}$$

$$\frac{\partial\langle V_\theta\rangle'}{\partial t} = -\hat{\mu}\langle V_\theta\rangle' + \alpha_3\langle V_\theta\rangle' E + \frac{\partial}{\partial x}\left(D_0 E\frac{\partial\langle V_\theta\rangle'}{\partial x}\right). \tag{11}$$

Note that the diffusion term and the $\alpha_1 E^2$ form of Eq. (10) together account for mode coupling to dissipation, and correspond to radial and poloidal drift coupling, respectively. Equation (10) is thus a "cartoon version" of a spatially integrated wave kinetic equation. The nonlocality of Eq. (10) is familiar from renormalized turbulence theories of tokamak turbulence,[12] where nonlinearities appear as diffusion operators. The nonlocal term of Eq. (11) is simply poloidal viscosity. Both transport terms are nonlinear (i.e., $D \approx D_0 E$), since diffusion is fluctuation induced.

Taken together, Eqs. (10) and (11) constitute a primitive K-ϵ model of turbulence and the L–H transition. Such familiar K-ϵ models fall midway between a full renormalized theory and primitive transport modeling. They treat the local fluctuation intensity as a field to be spatiotemporally evolved, and respect basic constraints, such as conservation of total energy between flow and fluctuations. The equations of a K-ϵ model have the structure of highly nonlinear reaction-diffusion equations, the solution of which are known to exhibit rich spatiotemporal behavior, such as propagating fronts.[13]

III. L–H TRANSITION PROPAGATION IN THE FLOW-FLUCTUATION MODEL

In this section, we consider the extension of the two-equation flow-fluctuation phase transition model[9] that incorporates the radial coupling given by Eqs. (10) and (11). This system of equations is a reaction-diffusion system with nonlinear diffusivity. The diffusivity allows propagating front solutions as well as diffusive damping. We will consider first the homogeneous case, with all coefficients independent of x, as it is simpler to extract the basic properties of the solutions. In this case, Eqs. (10) and (11) have the same fixed-point solutions as the zero-dimensional model. Apart from the trivial solution ($E=0$ and $\langle V_\theta\rangle'=0$), the two fixed points are (1) the L-mode fixed point,

$$E = \frac{\gamma_0}{\alpha_1} \quad \text{and} \quad \langle V_\theta\rangle' = 0; \tag{12}$$

and (2) the H-mode fixed point,

$$E=\frac{\hat{\mu}}{\alpha_3} \quad \text{and} \quad \langle V_\theta\rangle' = \pm\sqrt{\frac{\alpha_3\gamma_0-\hat{\mu}\alpha_1}{\alpha_3\alpha_2}}. \tag{13}$$

The local stability properties of these fixed points, which have been studied in Ref. 9, are modified by radial diffusion. The linear eigenvalues for the L-mode fixed point are $\gamma=-\gamma_0-\gamma_0 D_0 k^2/\alpha_1$ for the "fluctuation" mode, which is always heavily damped, and $\gamma=\gamma_0\Delta\epsilon-\gamma_0 D_0 k^2/\alpha_1$ for the "flow" mode. Here, k is the radial wave number and $\Delta\epsilon\equiv(\alpha_3/\alpha_1-\hat{\mu}/\gamma_0)$. The L-mode root becomes unstable if

$$\Delta\epsilon > \frac{D_0 k^2}{\alpha_1}. \tag{14}$$

Here, the transition is triggered by the flow instability when $\gamma>0$. In the case with split coupling, $\Delta\epsilon$ has to beat diffusive damping for the transition to occur. Equation (14) suggests that broad transition fronts are dynamically favored. In practice, $\Delta\epsilon$ is a function of x, and its x dependence will determine the width of the steep E_r' region. The transition condition can also be looked at in a different way—that is, as the determination of the radial correlation length. Using the expression suggested by mixing length estimates for α_1, we obtain

$$k_c^2 W_k^2 = \frac{\gamma_0 L_\perp^2}{D_0}\Delta\epsilon. \tag{15}$$

Note that the radial correlation length diverges at the critical point, as expected. For the H-mode fixed point, the local stability analysis indicates that both roots are stable with the added diffusive damping.

For the oversimplified but instructive case of constant coefficients, we can easily see that this system of equations exhibits propagating front solutions. We can look for solutions of Eqs. (10) and (11) that are functions of $\xi=x-ct$, where c is the front propagation velocity. These propagating fronts are the solution of the two nonlinear ordinary differential equations:

$$D_0\frac{d}{d\xi}\left(E\frac{dE}{d\xi}\right)-c\frac{dE}{d\xi}=\gamma_0 E-\alpha_1 E^2-\alpha_2\langle V_\theta\rangle'^2 E \tag{16}$$

and

$$D_0\frac{d}{d\xi}\left(E\frac{d\langle V_\theta\rangle'}{d\xi}\right)-c\frac{d\langle V_\theta\rangle'}{d\xi}=-\hat{\mu}\langle V_\theta\rangle'+\alpha_3\langle V_\theta\rangle' E. \tag{17}$$

We solve these two equations as an eigenvalue problem, with c being the eigenvalue and with boundary conditions asymptoting to the H-mode root for $\xi\to-\infty$ and to the L-mode solution for $\xi\to+\infty$. Thus, the solution of Eqs. (16) and (17) is a moving shearing front that "eats" into the fluctuations and pushes the H mode into the plasma core. In Fig. 1, we plot a particular solution as an illustration. For a fixed value of the parameters, this solution is not unique. An infinite sequence of solutions can be found, each with a different value of c and radial structure of the front. This situation is typical of diffusion-reaction equations. Indeed, a standard problem for this type of equation is to determine which of the possible solutions of the wave propagation equations is the actual solution of the partial differential equation for a given set of initial conditions. Alternatively, the problem is to find the front velocity (i.e., eigenvalue) of the solution of Eqs. (10) and (11) for this set of initial conditions. To address this issue analytically, a simplification of the initial system of equations, Eqs. (10) and (11), is needed.

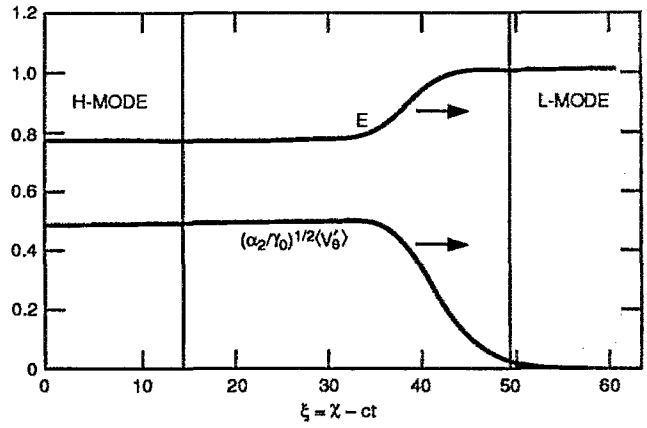

FIG. 1. Self-similar front propagation solution of Eqs. (16) and (17) with boundary conditions: the H-mode root for $\xi\to-\infty$ and the L-mode solution for $\xi\to+\infty$.

Therefore, by neglecting the diffusion term in the fluctuation equation (i.e., typically $\gamma_0\gg k^2 D_0$), the fluctuation level is

$$E=\frac{\gamma_0-\alpha_2\langle V_\theta\rangle'^2}{\alpha_1}. \tag{18}$$

As a result, the model is reduced to a single, albeit highly nonlinear, evolution equation for the local velocity shear,

$$\frac{\partial\langle V_\theta\rangle'}{\partial t}-\frac{\partial}{\partial x}\left[\frac{D_0\gamma_0}{\alpha_1}\left(1-\frac{\alpha_2\langle V_\theta\rangle'^2}{\gamma_0}\right)\frac{\partial\langle V_\theta\rangle'}{\partial x}\right]$$

$$=\gamma_0\Delta\epsilon\langle V_\theta\rangle'-\frac{\alpha_2\alpha_3}{\alpha_1}\langle V_\theta\rangle'^3. \tag{19}$$

This equation is similar to the Kolmogorov–Petrovsky–Piskunov[14] and to the Fisher equation,[15] with a nonlinear diffusion term. For this equation, we can now also look for propagating solutions by setting $\xi=x-ct$. The corresponding ordinary differential equation (in dimensionless variables) is

$$c_F\frac{dU}{d\xi}+\frac{d}{d\xi}\left[\left(1-\frac{\alpha_1\Delta\epsilon}{\alpha_3}U^2\right)\frac{dU}{d\xi}\right]+\Delta\epsilon\, U(1-U^2)=0, \tag{20}$$

where $U\equiv\langle V_\theta\rangle'/\sqrt{\Delta\epsilon}$, $c_F\equiv c/(\gamma_0\sqrt{D_0/\alpha_1})$, and the length, ξ, is normalized to the characteristic radial length, $L_D=\sqrt{D_0/\alpha_1}$.

Equation (20) can be interpreted as the motion of a particle in a potential field.[16] By defining the potential, F, as

$$F\equiv-\frac{1}{2}\Delta\epsilon\, U^2+J_0\epsilon\frac{1}{4}U^4, \tag{21}$$

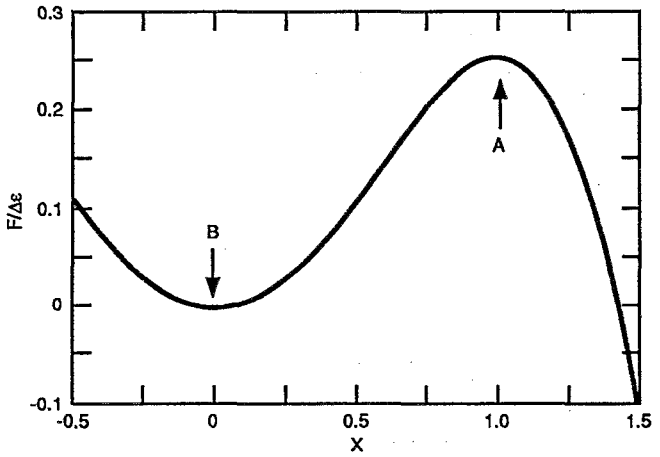

FIG. 2. Potential energy of a particle motion problem equivalent to the self-similar front propagation described by Eq. (20).

and identifying U with the particle position, $X(t)$, and ξ with time, t, Eq. (20) can be rewritten as a one-dimensional (1-D) nonlinear mechanics problem; i.e.,

$$\frac{d}{dt}\left(m(t)\frac{dX}{dt}\right)+c_F\frac{dX}{dt}-\frac{\delta F}{\delta X}=0. \tag{22}$$

This equation describes the motion of a particle with a time-dependent mass, $m(t)\equiv 1-\alpha_1\,\Delta\epsilon\,X(t)/\alpha_3$, subject to a frictional force, c_F, within a potential field, F. The form of the potential is plotted in Fig. 2. The eigenvalue problem is equivalent to determining the frictional force, c_F, which must be applied to the particle initially at position A (i.e., an H-mode root) so that it comes to rest at position B (L-mode root) with no oscillations around the position B. Note that in this problem, the mass of the particle decreases at the same time that it is accelerating downhill. This mechanical analogy allows considerable physical insight into the problem but also illustrates the difficulties encountered in practical calculations. To start the motion, the particle requires an infinitesimal push from A. Numerically, the push is never infinitesimal, and the solution depends on this initial push. Near the critical point, the initial condition determines the solution.

In the phase space $(U,dU/d\xi)$, Eq. (20) has two stationary points: (0,0), associated with the L-mode solution, and $(0,\pm 1)$, associated with the two H-mode roots. The linear stability analysis identifies the latter with a saddle point, and the L mode can be either a stable node, for $c_F^2>4\,\Delta\epsilon\equiv c_{\min}^2$, or a stable spiral, for $c_F^2<c_{\min}^2$. For a stable node, the front smoothly connects the H mode on the outside with the L-mode solution inside [Fig. 3(a)], while for a stable spiral, the front oscillates when connecting to the L mode [Fig. 3(b)]. It can be proven[17] that for initial conditions that are nonzero on a finite interval in x, the actual velocity of the front selected is the minimum value and is the value for a stable node—that is, $c_F=c_{\min}$. This is the value of the friction (in the particle motion analogy) that brings the particle to rest at point B (Fig. 2). This velocity is

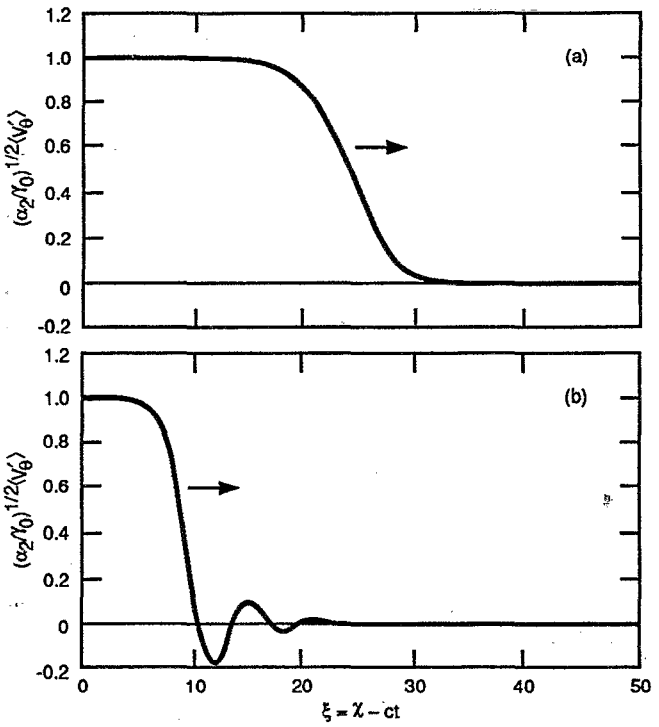

FIG. 3. Front propagation solution for the single-equation problem, Eq. (20): (a) For $c_F>c_{\min}$ and (b) for $c_F<c_{\min}$.

$$c=2\gamma_0\left(\frac{D_0}{\alpha_1}\right)^{1/2}\sqrt{\frac{\alpha_3}{\alpha_1}-\frac{\hat{\mu}}{\gamma_0}}\approx 2\,\frac{W}{L_\perp}\,(W\gamma_0)\sqrt{\Delta\epsilon}. \tag{23}$$

In this, we have approximated the turbulent diffusivity by $D_0\approx W^2\gamma_0$. Here, W is the spectral width W_k. Equation (23) shows that the front velocity is a hybrid of the turbulence velocity, $\gamma_0 W$, and of how much the local L–H threshold has been exceeded, $\Delta\epsilon\propto\sqrt{P-P_{\rm th}}$.[18] Near the critical point, the velocity of the front is small and the transition primarily diffuses inward. For $P\gg P_{\rm th}$, the velocity of the front is large, and it propagates nondiffusively.

An alternative way to analyze Eq. (19) is to study the evolution of the leading edge of the front. At the leading edge, the solution has low amplitude, so that the equation can be linearized. The front edge may be approximated by an exponential in x, $\langle V_\theta\rangle'\propto\exp(-\lambda x)$. The linear analysis leads to the following solution:

$$\lambda=\frac{c\alpha_1}{2D_0\gamma_0}\left(1\pm\sqrt{1-4\,\frac{\gamma_0^2 D_0}{c^2\alpha_1}\,\Delta\epsilon}\right). \tag{24}$$

To avoid oscillations in x, $c\geqslant 2\gamma_0\sqrt{D_0\,\Delta\epsilon/\alpha_1}$. This is the same condition as that for a stable node. Furthermore, when c reaches its minimum value and satisfies Eq. (23), $\lambda=\sqrt{\alpha_1\,\Delta\epsilon/D_0}$. Therefore, the characteristic scale length of the front, $\Delta_{\rm front}\approx 1/\lambda$, is

$$\Delta_{\rm front}\approx\sqrt{\frac{D_0}{\alpha_1\,\Delta\epsilon}}\approx\frac{W}{L_\perp}\,\frac{1}{\sqrt{\Delta\epsilon}}\,W. \tag{25}$$

The front scale length is the same as the transition layer correlation length, $1/k_c$, given by Eq. (15), and diverges at

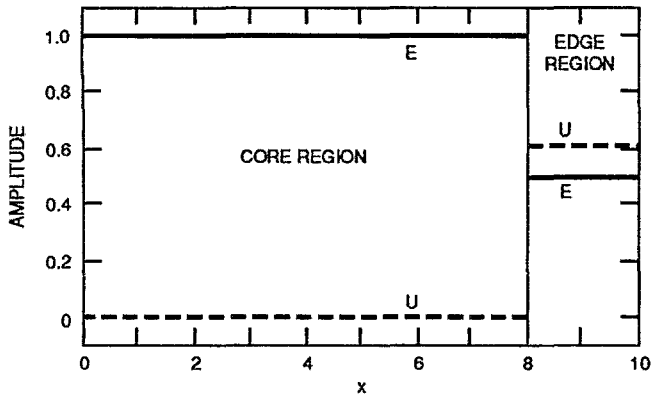

FIG. 4. Initial conditions for the H-mode front propagation from the edge into the L-mode region described by Eqs. (10) and (11).

the critical point. Having calculated the front velocity, we can determine its transit time, τ_T, which depends on the penetration length, L, that is the radial extent of the region with $\Delta\epsilon>0$, and is given by

$$\tau_T \approx \frac{L}{c} = \frac{L}{2\gamma_0}\sqrt{\frac{\alpha_1}{D_0\,\Delta\epsilon}} \approx \frac{1}{2\gamma_0}\frac{LL_\perp}{W^2}\frac{1}{\sqrt{\Delta\epsilon}}. \tag{26}$$

For the two-equation model with x-dependent coefficients, it is not possible to perform a similar analytical study, as has been done for Eq. (19). However, we can solve these equations numerically as an initial value problem and test how much of the information obtained from the analysis of Eq. (19) can be applied to the two-equation model. The initial value problem can be formulated in the following way. We start with a H-mode-type solution near the plasma edge and an L-mode solution everywhere else (Fig. 4). Then, Eqs. (10) and (11) are solved numerically using the finite difference partial differential equation solver PDE2D[19] on a rectangular domain. First, we consider the case with constant coefficients. Front propagation solutions are always found above the critical point, with propagation dominating over diffusion for all cases considered (Fig. 5). The front velocity agrees well with the single-equation result, Eq. (23), and exhibits the characteristic $\sqrt{\Delta\epsilon}$ dependence (Fig. 6).

When the system of equations has radially dependent coefficients, the front velocity is not a constant, and the front solution is no longer self-similar. The numerical results show that the system adapts rapidly to the local value of the parameters and that the instantaneous velocity has a similar dependence on the local parameters, as given by Eq. (19) (Fig. 6). For spatially varying parameters, the front velocity diverges from $\sqrt{\Delta\epsilon}$ near the critical point. This can be understood by recognizing that arbitrarily close to the critical point x_{front}, $\Delta\lambda_{\text{front}}$ will exceed the scale for variation of the coefficients. At a radial position near where $\Delta\epsilon=0$ (i.e., where locally the parameters go from supercritical to subcritical), the front velocity vanishes. The point at which the front actually stops is consistently at a value of $\Delta\epsilon$ somewhat greater than zero. This may be understood from the definition of the position of the front, which we take to be the middle of the propagating transition. If the coefficients change rapidly with x, $[(d\Delta\epsilon/dx)/(k_c\,\Delta\epsilon)\gg 1]$, there is some evidence that the front may overshoot the neutral point and then relax back. The numerical results also show that the steepness of the front and the front height are functions of $\Delta\epsilon$, in good agreement with the homogeneous single-equation results.

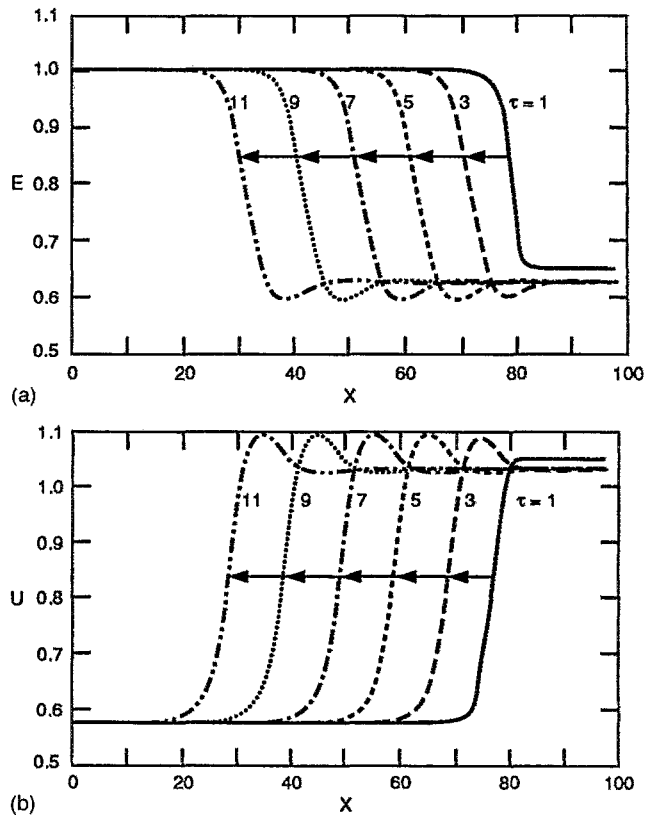

FIG. 5. Front propagation solution for the two equation model, Eqs. (10) and (11), with the parameters $\alpha_3/\alpha_1=1.4$, $\mu/\mu_0=1$, and $D_0=0.01$. (a) Fluctuation level profiles for a series of times; (b) U profiles for the same times. Note the propagation of the self-similar front inward as time advances.

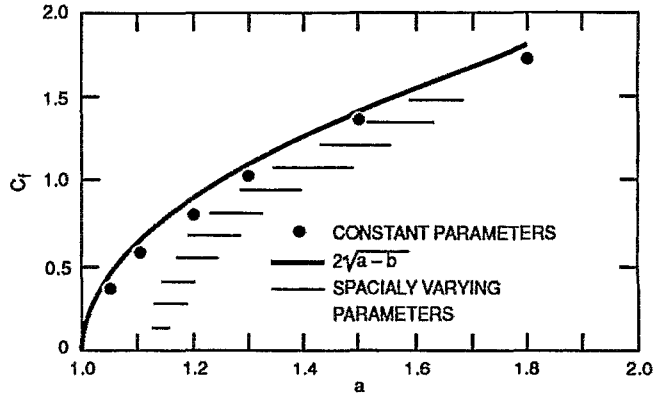

FIG. 6. Front velocity (c_F) for Eqs. (10) and (11) with $\mu/\gamma_0=1$, $D_0=0.01$, and $\alpha_3/\alpha_1=a$. The circles indicate different values of a, with that value held constant over x. The lines indicate a varying with x, with the curve being the analytic result.

IV. FLOW-FLUCTUATION-∇P_i MODEL

In the dynamics of the L–H transition, the ion pressure gradient, ∇P_i, plays an essential role.[11] The ∇P_i couples to the phase transition model in several ways. In particular, through the diamagnetic drift, ∇P_i contributes to the $\mathbf{E}\times\mathbf{B}$ shear velocity, which is no longer identical to the poloidal shear flow. Depending on the nature of the turbulence, ∇P_i also contributes to the turbulence drive through the gradient of the ion temperature, dT_i/dr, and/or the density gradient, dn/dr. Since changes on the turbulence level modify the transport, a transport equation for the evolution of ∇P_i is also needed.

A local phase transition model for the L–H transition incorporating the ∇P_i evolution was given in Ref. 11. The main consequences of the inclusion of ∇P_i in the phase transition model are (1) the existence of a quenched fluctuation fixed point, with E_r dominated by ∇P_i, which may have direct relevance to the experimental observations of the H mode; and (2) the appearance of broken symmetry in the H-mode state due to the preferred direction in the shear flow.[11] In this section, we extend the L–H transition front propagation model of Sec. III by including the effect of ∇P_i. For the extended model, the equations are

$$\frac{1}{2}\frac{\partial E}{\partial t}=\bar{\gamma}_0 NE-\alpha_1 E^2-\alpha_2\langle V_E'\rangle^2 E+\frac{\partial}{\partial x}\left(D_0 E\frac{\partial E}{\partial x}\right), \tag{27}$$

$$\frac{\partial\langle V_\theta'\rangle}{\partial t}=-\mu\langle V_\theta'\rangle+\alpha_3 E\langle V_E'\rangle+\frac{\partial}{\partial x}\left(D_0 E\frac{\partial\langle V_\theta'\rangle}{\partial x}\right), \tag{28}$$

$$\frac{\partial N}{\partial t}=-\alpha_5 N-\alpha_4 NE+\Gamma+\frac{\partial}{\partial x}\left(D_0 E\frac{\partial N}{\partial x}\right). \tag{29}$$

Here, we assume that the linear growth rate is proportional to the pressure gradient, $\gamma_0\equiv\bar{\gamma}_0(-dP_i/dr)(L_\perp/P_i)$, and we have introduced a symbol for the normalized pressure gradient, $N\equiv(-dP_i/dr)(L_\perp/P_i)$. In the pressure evolution equation, Γ is proportional to the energy flux from the plasma core and can be directly related to the power input. Also, $\alpha_4=\chi_1/W_k^2$, where $\chi_1 E$ is the anomalous diffusivity induced by the turbulence; and $\alpha_5=\chi_0/L_\perp^2$, where χ_0 is the neoclassical diffusivity.

To complete the set of equations, we need a relationship between the flow gradients and N. The poloidal flow velocity and the $\mathbf{E}\times\mathbf{B}$ velocity are related by

$$\langle V_\theta\rangle=\langle V_E\rangle-\frac{1}{eB_z n_e}\frac{dP_i}{dr}. \tag{30}$$

Since we want to avoid complications forced by considering the separate evolution of density and ion temperature, we assume (as in Ref. 11) that the density gradient dominates ∇P, and so the relation between poloidal and $\mathbf{E}\times\mathbf{B}$ shear flow is

$$\langle V_\theta\rangle'=\langle V_E\rangle'-\frac{\rho_s c_s}{L_\perp^2}N^2. \tag{31}$$

In this case, $N\equiv(-dn/dr)(L_\perp/n)$, and the ion temperature is assumed to be constant with time.

To carry out the numerical calculations, it is useful to write Eqs. (27)–(29) in the dimensionless form by setting

$$\tilde{E}\equiv\frac{\alpha_1 E}{\bar{\gamma}_0},\quad V\equiv\sqrt{\frac{\alpha_2}{\bar{\gamma}_0}}\langle V_E\rangle',\quad U\equiv\sqrt{\frac{\alpha_2}{\bar{\gamma}_0}}\langle V_\theta\rangle',$$
$$\tau=\bar{\gamma}_0 t,\quad X=\frac{x}{L_D}. \tag{32}$$

The L–H transition front propagation model is then described by four dimensionless equations:

$$\frac{\partial\tilde{E}}{\partial\tau}=\tilde{E}N-\tilde{E}^2-V^2\tilde{E}+\frac{\partial}{\partial X}\left(\tilde{E}\frac{\partial\tilde{E}}{\partial X}\right), \tag{33}$$

$$\frac{\partial U}{\partial\tau}=a\tilde{E}V-bU+\frac{\partial}{\partial X}\left(\tilde{E}\frac{\partial U}{\partial X}\right), \tag{34}$$

$$\frac{\partial N}{\partial\tau}=-A\tilde{E}N-BN+Q+\frac{\partial}{\partial X}\left(\tilde{E}\frac{\partial N}{\partial X}\right), \tag{35}$$

$$U=V-\alpha N^2. \tag{36}$$

Here, we have introduced six dimensionless parameters:

$$a\equiv\frac{\alpha_3}{\alpha_1},\quad b\equiv\frac{\mu}{\bar{\gamma}_0},\quad A\equiv\frac{\chi_1}{\bar{\gamma}_0 W_k^2}, \tag{37}$$

$$B\equiv\frac{\chi_0}{\bar{\gamma}_0 L_\perp^2},\quad Q\equiv\frac{\Gamma}{\bar{\gamma}_0 L_\perp\langle P_i\rangle},\quad \alpha\equiv\frac{c_s\rho_s}{L_\perp^2}\sqrt{\frac{\alpha_2}{\bar{\gamma}_0}}. \tag{38}$$

Equations (33)–(36) are solved numerically using the finite difference partial differential equation solver PDE2D[19] on a rectangular domain. The equations are inhomogeneous in x, and the boundary conditions are set to be periodic. The most accurate numerical scheme in PDE2D is utilized, and the solutions are checked for both spatial and temporal convergence. The radial domain was divided into two regions: edge and core. The edge was characterized by a higher driving (larger gradients at the edge) and higher Reynolds stress (i.e., a large edge gradient of the fluctuation envelope).

The numerical solutions can be classified into two extreme types: (1) propagating front solutions, which are very similar to the ones discussed in Sec. III; and (2) uniform transitions, in which case there is no radial propagation and the L–H transition occurs uniformly at all radial locations. The most important parameter characterizing these two types of solutions is α. Depending on the parameters, combinations of these two types of solutions are found with a rich variety of dynamics. Here, we consider the two extreme limits.

Propagating front solutions, like the ones described in Sec. III, exist only for small values of the parameter α. In this case, the sheared radial electric field is dominated by poloidal sheared flow. The fronts propagate nondiffusively, with propagation beating the simple diffusion speed for all cases tested above the transition threshold with α small enough. In Fig. 7, the poloidal shear flow, the fluctuation level, and the pressure gradient profile are shown at five different times after the edge transition. We can see the shear flow profile propagating inward. The more familiar pressure

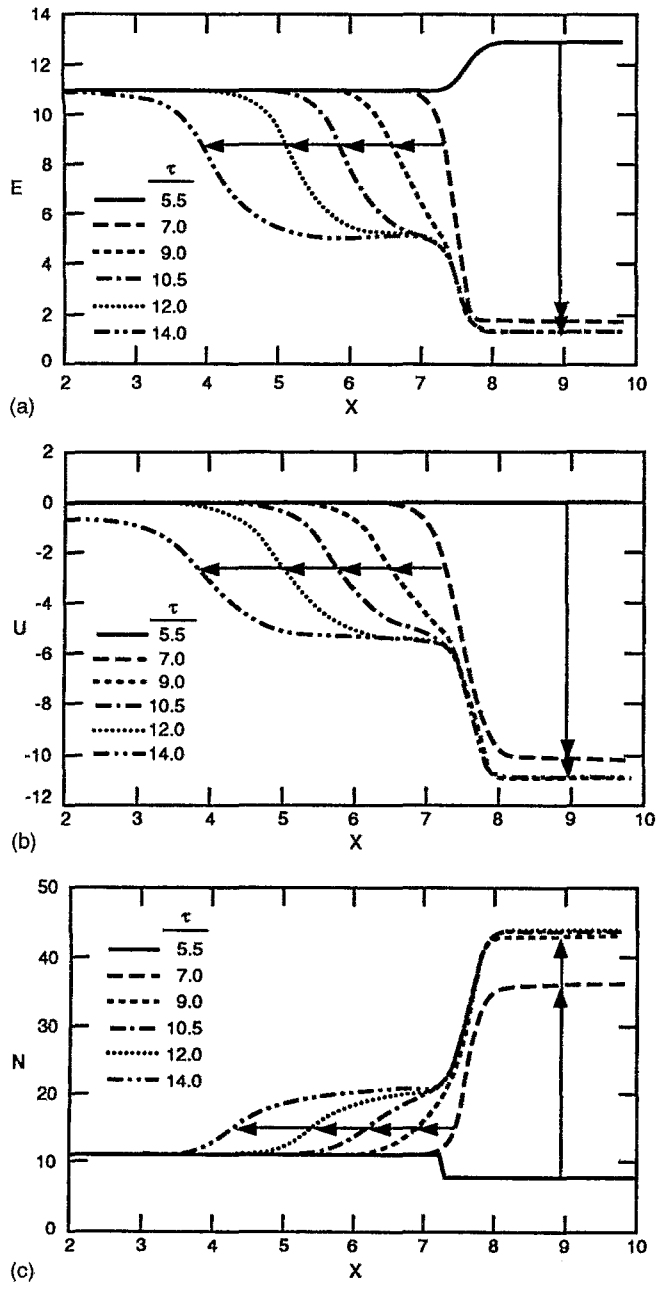

FIG. 7. Front propagation solution for the three-equation model, Eqs. (33)–(36). The parameters for this case are $Q=10.2$, $D_0=0.01$, $a_{\text{inside}}=0.6$, $a_{\text{edge}}=1.2$, $b=0.5$, $A=3$, $B=0.001$, and $\alpha=0.000\,01$. (a) Profiles of the fluctuation level, E, at successive times; (b) U profiles; (c) N profiles.

profiles are shown in Fig. 8 at the same times during the transition as in Fig. 7. The front propagation velocity, c_F, is given in dimensionless form by

$$c_F=2\sqrt{a\sqrt{\frac{Q}{A}}-b}. \tag{39}$$

This corresponds to the propagation velocity given in Eq. (25), with $\Delta\epsilon = a\sqrt{Q/A} - b$ for this variant of the model. The front velocity goes to zero at the critical point, $\sqrt{Q_{\text{crit}}/A} = b/a$. Equation (39), derived in the single-equation limit (Sec. III), agrees well with the numerical results for the propagating front solution of the three-equation model (Fig.

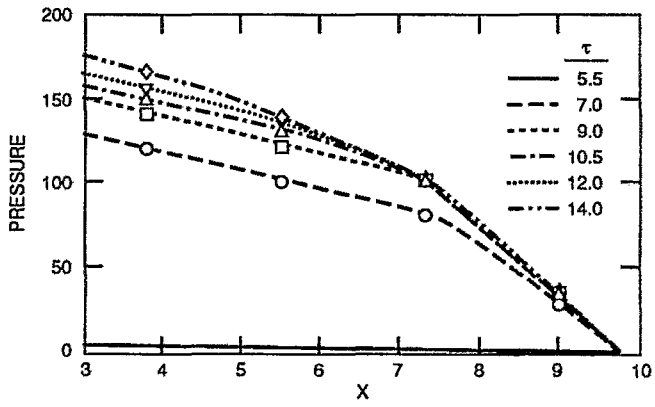

FIG. 8. Radial pressure profiles for the transition shown in Fig. 7.

9). If a smooth x dependence is included in the coefficients of the basic model, the front stops propagating when the velocity becomes zero—that is, the local parameters pass from supercritical to subcritical values.

The spatially uniform L–H transition always exists for $\alpha\neq 0$. This is in contrast to the two-equation model ($\alpha=0$), where there is no seed flow to start the transition, even if the core region is supercritical. For $\alpha\neq 0$, the pressure gradient gives a local diamagnetic seed flow and the transition can always be triggered. However, for small values of α the propagating front can pass through a particular radius before the local transition occurs there, as discussed above. In this case, the H-mode solutions are characterized by a strong or even a dominant contribution from the pressure gradient to the sheared radial electric field. Because the growth rate and Reynolds stress are larger at the edge, the transition is first triggered in the edge region (Fig. 10). This is followed by a uniform transition at all radial locations in the core that are locally supercritical. Both in the core and at the edge, the transition is triggered by the dynamo instability of the sheared poloidal flow, i.e., $\Delta\epsilon>0$. Note that the simultaneous transition within the core region, which is actually local in each radial location, gives the appearance of a nonlocal process. This is because the edge transition seems to propagate at an arbitrarily large velocity into the core region. The characteristic time scale for the transition, τ_f, is essentially the

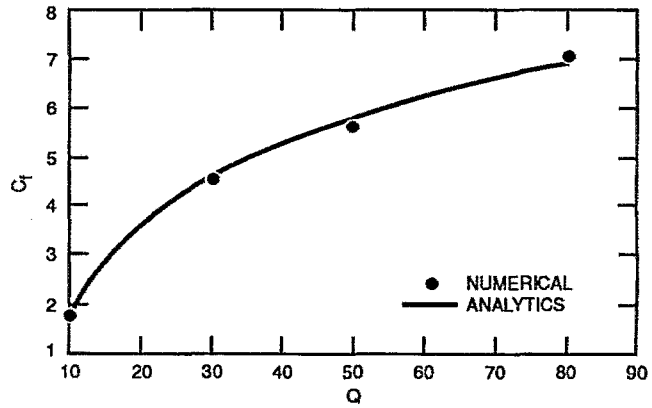

FIG. 9. Front velocity (c_F) as a function of Q/A for Eqs. (33)–(36). The parameters are the same as in Fig. 7, except for Q/A, which is varied.

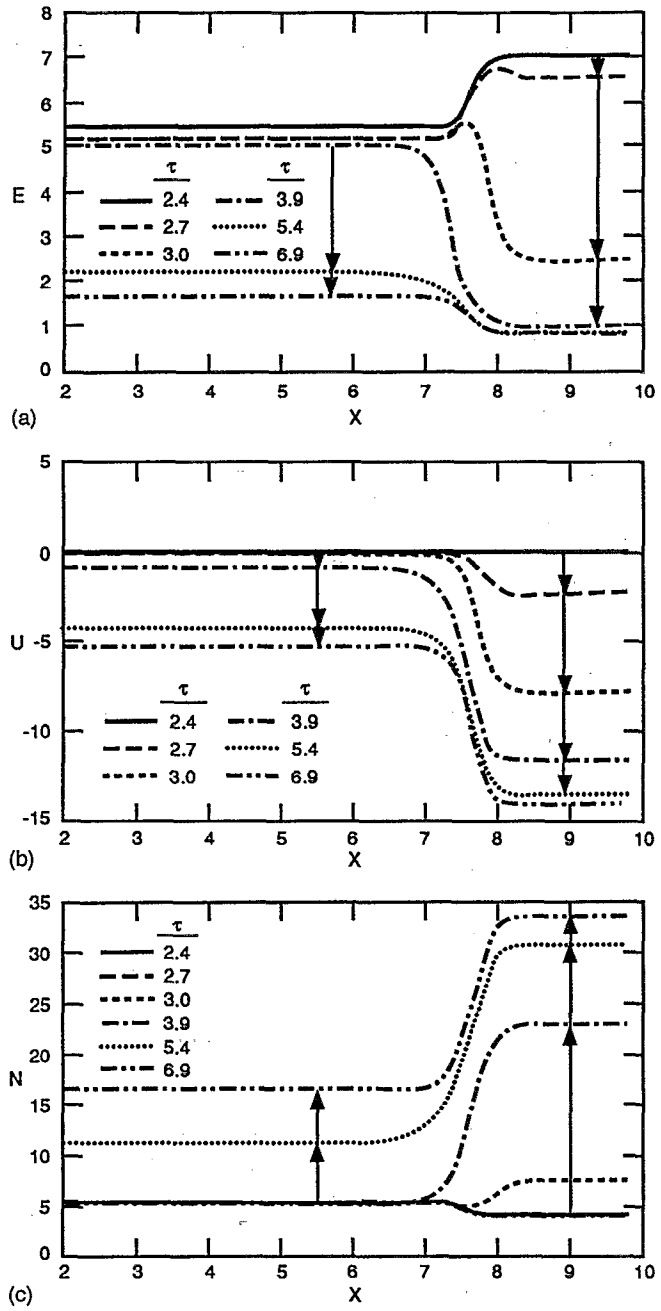

FIG. 10. Uniform transition for Eqs. (33)–(36). The parameters are the same as those in Fig. 7, except that $Q=20.2$ and $\alpha=0.001$. (a) Profiles of the fluctuation level (E) at successive times: (b) U profiles; (c) N profiles.

time taken for the electric field shear to build up and suppress the fluctuations. Assuming that the transition is from a supercritical L mode to H mode, the transition time is

$$\tau_f \approx \frac{1}{\bar{\gamma}_0(a\sqrt{(Q/A)}-b)} \ln\left(\frac{\langle V_\theta\rangle'|_H}{\langle V_\theta\rangle'|_L}\right) \approx \frac{1}{\bar{\gamma}_0(a\sqrt{(Q/A)}-b)} \times \ln\left(\frac{A[a^2(Q/A)-b^2]^{1/2}(a\sqrt{(Q/A)}-b)}{a^{1/2}b^{3/2}\alpha Q}\right). \quad (40)$$

This time scale diverges near the critical point, $\sqrt{Q_{\mathrm{crit}/A}} = b/a$, as it should. At each radial position, this result agrees with the numerical calculations (Fig. 11). The duration of the

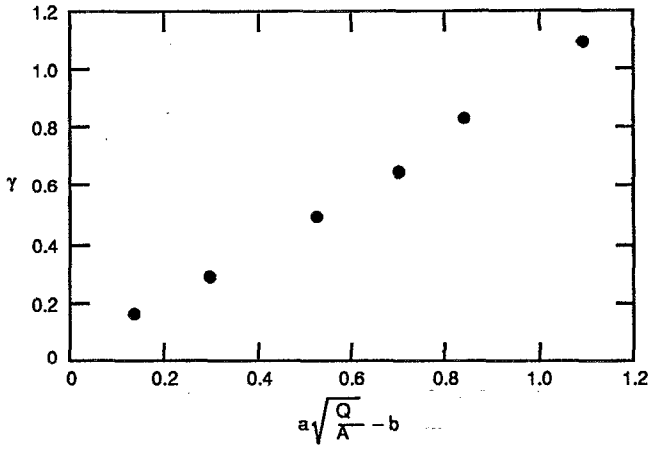

FIG. 11. Transition time scale for the uniform transition. The parameters are the same as in Fig. 9, except for the varying Q/A.

transition depends on the nonlinear evolution. However, this phase has a much shorter time scale than Eq. (40) and seems to be controlled by the evolution of E. Therefore, the relative magnitude of the front transit time, τ_T, and the fluctuation reduction time is

$$\frac{\tau_T}{\tau_f} = \frac{1}{2}\frac{LL_\perp}{W^2}\sqrt{a\sqrt{\frac{Q}{A}}-b}\left[\ln \times\left(\frac{A[a^2(Q/A)-b^2]^{1/2}(a\sqrt{(Q/A)}-b)}{a^{1/2}b^{3/2}\alpha Q}\right)\right]^{-1}. \quad (41)$$

Hence, front propagation dominates for power densities near the threshold values and for very small values of α. A particularly interesting case is when the input power is large enough to trigger a uniform transition to the quenched-fluctuation state. In this case, the edge transition always occurs first and exhibits the usual characteristics. However, the uniform transition in the core region can occur without generation of sheared poloidal flow. This type of uniform transition is relevant only for very high-power levels. Indeed, for such levels there is no L-mode state solution in the present model, and the interpretation of this result is unclear.

V. DISCUSSION AND CONCLUSIONS

In this paper, we have explored the spatiotemporal propagation dynamics of L–H transitions fronts. The principal results of this paper are as follows.

(1) The phase transition model (with ∇P_i) of the L–H bifurcation has been extended to include spatial coupling effects and can describe propagating transition fronts.

(2) The flow-fluctuation model exhibits spatially propagating front solutions. The fronts propagate into locally supercritical regions once a seed flow has been established.

(3) The front propagation velocity is

$$V_F = 2\frac{W}{L_\perp}(\gamma_0 W)\sqrt{\Delta\epsilon} \approx \frac{2W}{\sqrt{\tau_E\tau_f}},$$

where $\Delta\epsilon>0$ is the local supercriticality condition, τ_E is the confinement time, and τ_f is the local transition time. Note that front propagation is determined by transport ($D\approx\gamma_0 W^2$) and the local supercritical bifurcation instability. The time scale for VH-mode development is not determined solely by transport.

(4) Front propagation ceases when $\Delta\epsilon\rightarrow 0$ locally. This point is determined by L-mode profiles.

(5) When the pressure gradient evolution is included, a uniform fluctuation reduction or quench can occur. The route to transition depends on the ratio τ_T/τ_f, the ratio of the front transit time τ_T to the local fluctuation reduction time τ_f. Typically, when $\langle V_\theta\rangle'>\langle V_d\rangle'$, $\tau_T<\tau_f$ so the transition occurs via direct fluctuation reduction.

Having developed the basic theory of spatiotemporally propagating transition fronts, it is now possible to address the issues concerning the VH mode raised earlier. First, the VH mode develops by a spatially propagating (i.e., convective) transition instability. The dynamics of this instability are a hybrid of local transport and the local phase transition instability. Propagation can occur either slowly (i.e., $\tau_T>\tau_f$), in the form of a localized but moving front, or rapidly (i.e., $\tau_f>\tau_T$) in the form of a "nonlocal" collapse. Second, both $\langle V_\theta\rangle'$ and $\langle V_d\rangle'$ contribute to the spatiotemporally evolving $\langle V_E\rangle'$. For $\tau_T>\tau_f$, the electric field is primarily the result of rotation. For $\tau_f>\tau_T$, $\langle V_d\rangle'$ dominates. Also, since the spatially localized transition model indicates that the finite $\langle V_\theta\rangle'$ stage is usually of limited duration, it follows that the $\langle V_\theta\rangle'\neq 0$ layer should appear as an "attached wake," which lags behind (but moves with) the local transition front. In the case of a "nonlocal collapse," the extent of this $\langle V_\theta\rangle'$ wake shrinks. Thus, detecting poloidal rotation associated with VH-mode evolution is most feasible when $P\geq P_{\text{crit}}$, using a multichannel (in space) charge exchange recombination (CER) system. Note that toroidal rotation (V_ϕ) is not *a priori* necessary for a spatially propagating transition. This is consistent with the fact that a VH-mode-like regime has been achieved on JET and TUMAN-3. Third, the extent of the enhanced confinement zone is determined by the radial width of the locally supercritical region (i.e., $\Delta\epsilon>0$). Note that this criterion naturally favors conditions of modest density and high ion temperature (to minimize magnetic pumping), as well as peaked profiles (to maximize drive). Such conditions are typical of VH-mode discharges. It is worthwhile to point out that the front propagation is initialized by a small, strongly supercritical (to L–H transition) region at the edge. This triggers a propagating transition front, which then moves into a weakly supercritical core. The strongly supercritical edge is created by boundary effects or strong fluctuation energy gradients—both typical of L-mode edge plasmas. It follows that the VH mode should develop from the "seed" region to the periphery of the power deposition region.

Having discussed the general properties of the propagation of transport barriers, we can estimate the propagation velocity for particular environmental conditions. We consider a DIII-D discharge[20] of 1 MA with a toroidal magnetic field 1.2 T. The L-mode edge parameters for this discharge are $T_i=120$ eV, $n_e=1\times10^{13}$ cm^{-3}, $L_\perp=2.7$ cm, and $\chi_{\text{eff}}\approx 2\times10^4$ cm^2/s. We assume that $L_s=180$ cm and $W=1$ cm. For JET,[21] the corresponding parameters are $T_i=400$ eV, $n_e=1\times10^{13}$ cm^{-3}, $L_\perp=2.7$ cm, and $\chi_{\text{eff}}\approx 4\times10^4$ cm^2/s. Here, we take $L_s=360$ cm and $W=1$ cm. Using these parameters, we can estimate the power threshold, the front propagation velocity, and the transition time. The values obtained are given in Table I. Note that by transition time we mean the rise time of the shear flow, not the fluctuation quench time.

TABLE I. Transition parameters.

	Power threshold	Transition time	Front propagation velocity
DIII-D	2.6 MW	4.7 ms	25 m/s
JET	2.3 MW	2.6 ms	47 m/s

While this model discussed above demonstrates the simplicity and generality of the propagating transition front phenomenon, it is not fully suitable for detailed quantitative comparison with data from DIII-D. This is because it omits the following factors:

(1) Toroidal velocity shear evolution and transport. Note that V_ϕ, as well as V_θ, influences E_r' evolution, and is the dominant contributor to E_r' in DIII-D;
(2) profile evolution due to fueling. This might mitigate the need for a large supercritical region; and
(3) local pressure gradient limitation due to the essential element of flux-surface triangularity, which allows access to the second-stable region. This is crucial for explaining why ELMs do not occur in the VH mode.

A more complete model, suitable for comparison with VH-mode data, will be discussed in a future publication.

We conclude by noting that all the examples and results discussed here are seeded with the intent of describing VH-mode-like phenomena, in which the transport barrier propagates and extends from the edge inward. However, we emphasize that this is not intrinsic to transport barrier dynamics, but is simply a consequence of initializing a seed shear flow or steep ∇P_i at the outer boundary. Initializing a steep ∇P_i in the confinement region, in turn, triggers an outward propagating barrier, as found in JT-60U. This phenomenon will be discussed further in future publications.

ACKNOWLEDGMENTS

We acknowledge stimulating discussions with K. Burrell, T. Osborne, J. G. Cordey, V. E. Golant, and S. Lebedev.

This work is supported by the U.S. Department of Energy through Grant No. DE-FG03-88-ER-53275 and under Contract No. DE-AC05-84OR21400 with Martin Marietta Energy Systems, Inc.

[1] F. Wagner, G. Becker, K. Behringer, D. Campbell, A. Eberhagen, W. Engelhardt, G. Fussmann, O. Gehre, J. Gernhardt, G. v. Gierke, G. Haas, M. Huang, F. Karger, M. Keilhacker, O. Klüber, M. Kornherr, K. Lackner, G. Lisitano, G. G. Lister, H. M. Mayer, D. Meisel, E. R. Müller, H. Murmann, H. Niedermeyer, W. Poschenrieder, H. Rapp, H. Röhr, F. Schneider, G. Siller, E. Speth, A. Stäbler, K. H. Steuer, G. Venus, O. Vollmer, and Z. Yü, Phys. Rev. Lett. **49**, 1408 (1982).
[2] H. Biglari, P. H. Diamond, and P. W. Terry, Phys. Fluids B **2**, 1 (1990).
[3] K. C. Shaing, Phys. Fluids B **4**, 171 (1992).

[4]K. H. Burrell, Plasma Phys. Controlled Fusion A **36**, 291 (1994).
[5]G. L. Jackson, J. Winter, T. S. Taylor, K. H. Burrell, J. C. DeBoo, C. M. Greenfield, R. J. Groebner, T. Hodapp, K. Holtrop, E. A. Lazarus, L. L. Lao, S. I. Lippmann, T. H. Osborne, T. W. Petrie, J. Phillips, R. James, D. P. Schissel, E. J. Strait, A. D. Turnbull, W. P. West, and the DIII-D Team, Phys. Rev. Lett. **67**, 3098 (1991).
[6]C. M. Greenfield, B. Balet, K. H. Burrell, M. S. Chu, J. G. Cordey, J. C. DeBoo, N. Deliyanakis, E. J. Doyle, R. J. Groebner, G. L. Jackson, S. Konoshima, D. P. O'Brien, L. Porte, C. L. Rettig, T. H. Osborne, H. St. John, A. C. C. Sips, G. M. Staebler, E. J. Strait, P. M. Stubberfield, T. S. Taylor, S. J. Thompson, K. Thomsen, A. D. Turnbull, and the JET and DIII-D Teams, Plasma Phys. Controlled Fusion B **35**, 263 (1993).
[7]M. V. Andrejko, L. G. Askinazi, V. E. Golant, V. A. Kornev, S. V. Lebedev, L. S. Levin, G. T. Razdobarin, V. V. Rozhdestvensky, A. S. Tukachinsky, and S. P. Jaroshevich, Plasma Phys. Controlled Fusion A **36**, 165 (1994).
[8]Y. Koide, M. Kikuchi, S. Ishida, M. Mori, S. Tsujī, N. Asakwa, Y. Kamada, T. Nishitani, Y. Kawano, T. Matae, T. Fujita, T. Fukuda, A. Sakasai, T. Kondoh, R. Yoshino, and Y. Neyatani, Plasma Phys. Controlled Fusion A **36**, 195 (1994).
[9]P. H. Diamond, Y-M. Liang, B. A. Carreras, and P. W. Terry, Phys. Rev. Lett. **72**, 2565 (1994).
[10]J. D. Murray, *Mathematical Biology* (Springer-Verlag, Berlin, 1989).
[11]B. A. Carreras, D. Newman, P. H. Diamond, and Y-M. Liang, Phys. Plasmas **1**, 4014 (1994).
[12]B. A. Carreras, L. Garcia, and P. H. Diamond, Phys. Fluids **30**, 1388 (1987).
[13]D. McComb, *The Physics of Fluid Turbulence* (Oxford University Press, Oxford, 1990).
[14]A. Kolmogorov, I. Petrovsky, and N. Piskunov, Bull. Univ. Moscou Sér. Int. Sec. A **1**, 1 (1937).
[15]R. A. Fisher, Ann. Eugenics **7**, 355 (1937).
[16]Y. Pomeau, Physica D **23**, 3 (1986).
[17]W. van Saarloos, Phys. Rev. A **37**, 211 (1988).
[18]B. A. Carreras, P. H. Diamond, Y-M. Liang, V. Lebedev, and D. Newman, Plasma Phys. Controlled Fusion A **36**, 93 (1994).
[19]G. Sewell, *Analysis of a Finite Element Method: PDE/PROTRAN* (Springer-Verlag, Berlin, 1990).
[20]P. Gohil, K. H. Burrell, E. J. Doyle, R. J. Groebner, J. Kim, and R. P. Seraydarian, Nucl. Fusion **34**, 1057 (1994).
[21]F. Tibone, B. Balet, J. G. Cordey, G. Carrigan, C. Sack, T. E. Stringer, and A. Taroni, Bull. Am. Phys. Soc. **36**, 2366 (1991).